



High-resolution Transmission Spectroscopy of Four Hot Inflated Gas Giant Exoplanets

Jiří Žák^{1,2} , Petr Kabáth¹ , Henri M. J. Boffin³ , Valentin D. Ivanov³ , and Marek Skarka^{1,2} 

¹Astronomical Institute, Czech Academy of Sciences, Fričova 298, 25165, Ondřejov, Czech Republic; 437396@mail.muni.cz

²Department of Theoretical Physics and Astrophysics, Masaryk University, Kotlářská 2, 61137 Brno, Czech Republic

³ESO, Karl-Schwarzschild-str. 2, D-85748 Garching, Germany

Received 2019 January 3; revised 2019 July 14; accepted 2019 July 15; published 2019 August 21

Abstract

The technique of transmission spectroscopy allows us to constrain the chemical composition of the atmospheres of transiting exoplanets. It relies on very high signal-to-noise spectroscopic (or spectrophotometric) observations and is thus most suited for bright exoplanet host stars. In the era of the *Transiting Exoplanet Survey Satellite*, Next Generation Space Telescope, and PLANetary Transits and Oscillations of stars (PLATO), more and more suitable targets, even for mid-sized telescopes, are discovered. Furthermore, a wealth of archival data is available that could become a basis for long-term monitoring of exo-atmospheres. We analyzed archival High Accuracy Radial velocity Planet Searcher (HARPS) spectroscopic time series of four host stars to transiting bloated gas exoplanets, namely WASP-76b, WASP-127b, WASP-166b, and KELT-11b, searching for traces of sodium (sodium doublet), hydrogen ($H\alpha$, $H\beta$), and lithium (670.8 nm). The archival data sets include spectroscopic time series taken during transits. Comparing in- and out-of-transit spectra we can filter out the stellar lines and investigate the absorption from the planet. Simultaneously, the stellar activity is monitored using the Mg I and Ca I lines. We detect sodium in the atmosphere of WASP-76b at a $7\text{--}9\sigma$ level. Furthermore, we report also at a $4\text{--}8\sigma$ level of significance the detection of sodium in the atmosphere of WASP-127b, confirming earlier results based on low-resolution spectroscopy. The data show no sodium nor any other atom at high confidence levels for WASP-166b nor KELT-11b, hinting at the presence of thick high clouds.

Key words: planetary systems – planets and satellites: atmospheres – planets and satellites: individual (WASP-76b, WASP-127b, WASP-166b, KELT-11) – techniques: spectroscopic

1. Introduction

Transmission spectroscopy has the power to probe the physical conditions in the atmospheres of exoplanets, as it allows for the detection of the various absorption features that are imprinted on the stellar light that passes through their atmospheres. Not surprisingly, the first detections of features in exo-atmospheres were made from space (Charbonneau et al. 2002; Vidal-Madjar et al. 2003), while ground-based transmission spectroscopy delivered its first secure detection of sodium in extrasolar atmospheres only about a decade ago (Redfield et al. 2008; Snellen et al. 2008b). If from space, only low-resolution spectroscopy can be used, from the ground, both low-resolution spectrophotometry and high-resolution spectroscopy can and have been used to detect atoms and molecules in the atmospheres of several exoplanets. In particular, in most recent years, high-resolution spectroscopy has been more and more successful. Moreover, Wyttenbach et al. (2015) used the High Accuracy Radial velocity Planet Searcher (HARPS) at the European Southern Observatory (ESO) 3.6 m telescope to be able to detect sodium in HD 189733b, demonstrating that spectrographs attached to moderate-size telescopes can also be used for this purpose. In the past only a handful of suitable, bright enough targets were available for such kind of study, but this is now changing rapidly with the discoveries from the *TESS* mission (Ricker et al. 2015; Kabáth et al. 2019). The high resolving power, i.e., $R \geq 40,000\text{--}60,000$, removes the need for a reference star that is at the same time close on sky to the target, and of similar brightness—two rarely met conditions that are limiting the low-resolution spectrophotometry studies. In contrast, the high resolving power solely requires accurate telluric correction and a careful analysis of the radial velocities of the star–planet

system (e.g., Astudillo-Defru & Rojo 2013; Wyttenbach et al. 2017).

Another advantage of high-resolution spectroscopy is its ability to resolve and characterize individual planetary absorption lines. In particular, the Na D lines are well suited for transmission spectroscopy due to the strong expected signal and the fact that they are very narrow features, in comparison to the broad molecular absorption bands of, e.g., CH_4 , H_2O , TiO , and VO .

If sodium, and in some cases, potassium measurements based on low-resolution spectra were reported (e.g., for some of the most recent ones, Sedaghati et al. 2016; Chen et al. 2017, 2018; Lendl et al. 2017; Murgas et al. 2017; Pallé et al. 2017; Pearson et al. 2019), only a few studies detected sodium using high-resolution transmission spectroscopy: Wyttenbach et al. (2017) registered strong absorption signal in WASP-49b. Using HARPS-N mounted on the Telescopio Nazionale Galileo (TNG), Casasayas-Barris et al. (2017) and Casasayas-Barris et al. (2018) concluded the presence of sodium in the atmospheres of WASP-69b and MASCARA-2b. Khalafinejad et al. (2018) tentatively detected sodium in WASP-17b using the MIKE instrument on the 6.5 m *Magellan* Telescope. Finally, Jensen et al. (2018) detected sodium and hydrogen in WASP-12b using the Hobby–Eberly Telescope and Deibert et al. (2019) found sodium in HAT-P-12b using the Subaru Telescope.

These are not the only elements to have been discovered in the atmospheres of exoplanets, as there are published detections of hydrogen (Ehrenreich et al. 2008; Lecavelier Des Etangs et al. 2010; Jensen et al. 2012), helium (Nortmann et al. 2018; Spake et al. 2018; Allart et al. 2018, 2019), calcium, scandium (Astudillo-Defru & Rojo 2013), TiO and VO (Désert et al. 2008; Sedaghati et al. 2017), CO (Snellen et al. 2008a), H_2O ,

Table 1
Properties of the Four Targets (Star and Planet) Considered in This Paper

	Parameters	WASP-76	WASP-127	WASP-166	KELT-11
Star	V mag	9.5	10.5	9	8
	Sp. Type	F7	G5	F9	G8/K0
	$M_s (M_\odot)$	1.46 ± 0.07	1.31 ± 0.05	1.19 ± 0.06	$1.438^{+0.061}_{-0.052}$
	$R_s (R_\odot)$	1.73 ± 0.04	1.33 ± 0.03	1.22 ± 0.06	$2.72^{+0.17}_{-0.17}$
	$T_{\text{eff}} (K)$	6250 ± 100	5750 ± 100	6050 ± 50	5370^{+51}_{-50}
	$\log g$	4.4 ± 0.1	3.9 ± 0.1	4.5 ± 0.1	$3.727^{+0.04}_{-0.046}$
	$M_p (M_{\text{Jup}})$	0.92 ± 0.03	0.18 ± 0.02	0.102 ± 0.004	$0.195^{+0.019}_{-0.018}$
Planet	$R_p (M_{\text{Jup}})$	$1.83^{+0.06}_{-0.04}$	1.37 ± 0.04	0.63 ± 0.03	$1.37^{+0.15}_{-0.12}$
	Period (days)	1.809886 ± 0.000001	4.178062 ± 0.000002	5.443526 ± 0.00001	$4.736529^{+0.000068}_{-0.000059}$
	Transit duration (days)	0.1539 ± 0.0008	0.1795 ± 0.0007	0.148 ± 0.008	$0.3051^{+0.0053}_{-0.0051}$
	Orbital semimajor axis (au)	0.33 ± 0.0005	0.052 ± 0.0005	0.0642 ± 0.0001	$0.06229^{+0.00088}_{-0.00076}$
	Orbital inclination (deg)	$88.0^{+1.3}_{-1.6}$	$88.7^{+0.8}_{-0.6}$	87.8 ± 0.6	$85.8^{+2.4}_{-1.8}$
	Reference	West et al. (2016)	Lam et al. (2017)	Hellier et al. (2019)	Pepper et al. (2017)

and CH₃ (Tinetti et al. 2007; Swain et al. 2008; Birkby et al. 2013). Some of these detections were disputed by Gibson et al. (2011) who discuss in great detail the complex systematics that affect the results, even those obtained from space. This issue was addressed in recent years by paying closer attention to the systematic effects (e.g., Sedaghati et al. 2015) and by introducing new stable instruments.

It is also important to note that there is a tremendous amount of archival spectra—obtained during transits for other purposes, such as measuring the spin–orbit alignment measurements via the Rossiter–McLaughlin (R–M) effect (Queloz et al. 2000)—that are available for further analysis. They can set the foundation of long-term exoclimate studies. Therefore, the method of high-resolution transmission spectroscopy from the ground is likely to become even more widely used than today, and to gain further importance for the characterization of exo-atmospheres.

Here we investigate the atmospheric chemistry of two inflated super Neptunes and two inflated hot Jupiters with archival HARPS data.⁴ We study the instrument systematics that can influence the results and the effects of the stellar activity (see Klocová et al. 2017 and Oshagh et al. 2018 for further discussion) using the calcium lines as activity indicators (Khalafinejad et al. 2017). This work is part of a larger effort to characterize systematically and uniformly a large number of exoplanetary atmospheres, and to shed more light onto their chemical composition. We also aim to identify interesting targets for CHaracterising ExOPlanets Satellite (CHEOPS) and James Webb Space Telescope (JWST) follow-up.

2. Data Sets and Their Analysis

2.1. Data Summary

Table 1 presents the main properties of our targets, while Table 2 shows the various data sets we used. For illustration purposes we show part of the spectrum around the sodium Na D region of each of our targets, along with the telluric spectrum in Figure 1.

WASP-76b. The HARPS data are covering three transit events, on 2012 November 11/12, 2017 October 24/25, and 2017 November 22/23. The total number of frames was 176 with 105 in-transit, and the exposure times were between 300 and 600 s.

WASP-127b. The HARPS data are covering two transit events during the nights of February 27/28 and 2017 March 19/20. The total number of frames was 82, of which 52 were in-transit.

WASP-166b. The HARPS data are covering three transits during the nights of January 13/14, March 3/4, and 2017 March 14/15. The total number of frames was 188, of which 112 were in-transit.

KELT-11b. The HARPS data are covering three transit events and four nights of out-of-transit on February 1/2 (transit), February 14/15, February 15/16 (transit), February 16/17, March 05/06, March 6/7 (transit), and 2017 March 7/8. The total number of frames was 342, of which 144 were in-transit.

2.2. Data Reduction

We retrieved the publicly available HARPS (Mayor et al. 2003) reduced spectroscopic data sets from the ESO Science data archive for the four planets WASP-76b, WASP-127b, WASP-166b, and KELT-11b (see Table 1). The retrieved data are fully reduced products obtained with the HARPS Data Reduction Software (DRS version 3.5). In more detail, each spectrum is provided as a merged 1D spectrum with 0.01 Å wavelength step. The reduced spectrum covers the wavelength range between 380 and 690 nm, and has a spectral resolution $R \approx 115,000$ corresponding to 2.7 km s^{-1} per resolving element. Spectra are corrected to the barycentric frame of reference. The sodium doublet is well-centered on the 16th order of HARPS.

2.3. Normalization

We obtained the radial velocities of the star (see below) from the FITS header of the spectra and subsequently shifted both during transit $f(\lambda, t_{\text{in}})$ and out of transit $f(\lambda, t_{\text{out}})$ frames to the stellar rest frame. We have made a cut of the region of interest and performed a normalization for the obtained spectra $f(\lambda, t_{\text{in}}) \rightarrow \tilde{f}(\lambda, t_{\text{in}})$ and $f(\lambda, t_{\text{out}}) \rightarrow \tilde{f}(\lambda, t_{\text{out}})$, where the tilde represents normalization. Normalization has been carried out using the standard IRAF routine *continuum*. More precisely, a Legendre polynomial has been used to perform the normalization of continuum regions without strong lines within the regions centered around the Na D lines (583–596 nm), H α (645–670 nm), H β (475–495 nm), and lithium (666–674 nm).

⁴ Data were obtained under program IDs 090.C-0540(F), 098.C-0304(A), and 0100.C-0750(A).

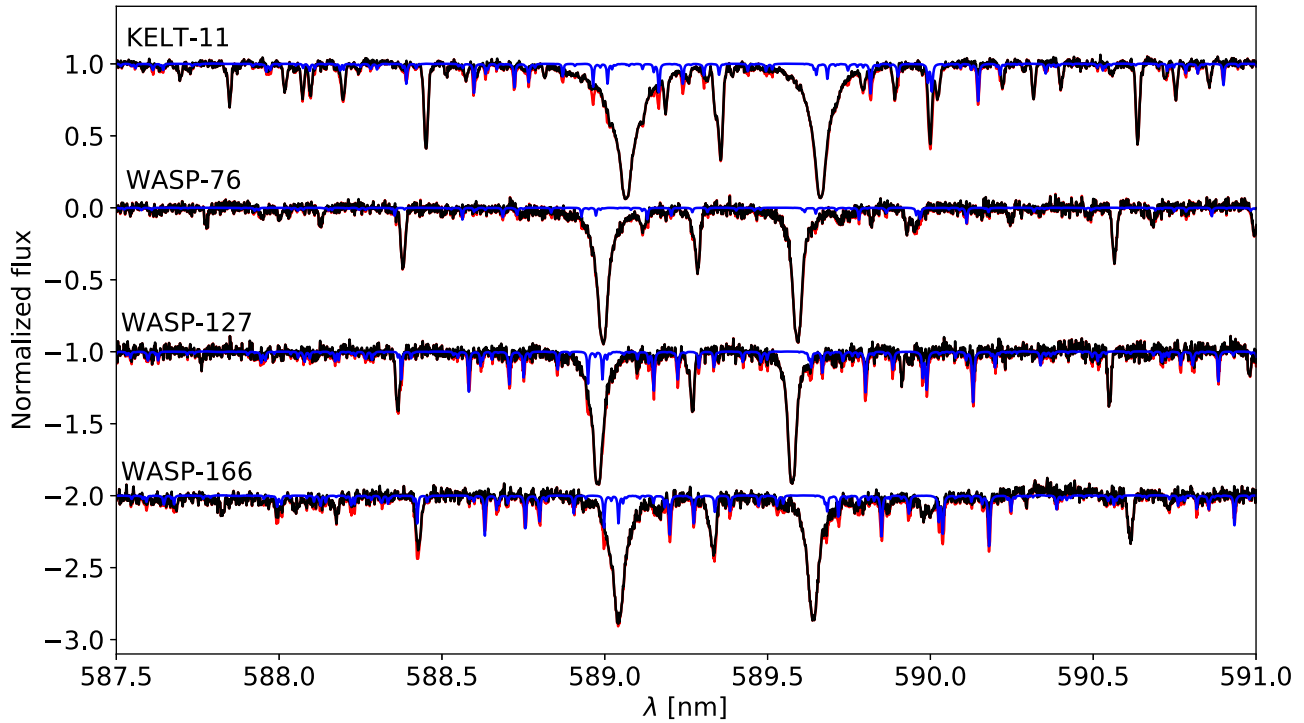


Figure 1. Illustration of the spectral region around the Na D lines for one selected example spectrum for each of our targets. The observed spectra in red are presented in the stellar reference frame during mid-transit. Telluric spectra are shown in blue. Observed spectra after telluric correction are presented in black.

Table 2
Observing Logs for All Four Data Sets

Date	No. Spectra	Exp. Time (s)	Airmass Range	Median S/N	S/N ^a
WASP-76					
2012 Nov 12	64 (40)	300	1.79–1.18–1.48	21.1–31.6	13.3–20.6
2017 Oct 25	49 (27)	400–600	1.75–1.18–2.10	32.1–55.8	18.7–34.2
2017 Nov 23	66 (40)	300–400	1.42–1.18–2.45	30.7–53.5	15.5–31.8
WASP-127					
2017 Feb 28	37 (22)	500	1.40–1.11–1.47	29.9–40.0	14.7–20.1
2017 Mar 20	45 (30)	500–600	1.98–1.11–1.55	26.4–38.2	14.0–19.5
WASP-166					
2017 Jan 14	75 (39)	300–350	2.37–1.01–1.17	20.0–52.8	11.0–33.0
2017 Mar 4	52 (39)	300–400	1.01–1.21–2.55	26.4–65.0	13.5–37.3
2017 Mar 15	66 (34)	350	1.17–1.01–2.35	18.8–55.3	8.6–29.9
KELT-11					
2017 Feb 2	37 (24)	300	1.42–1.11–1.08	81.2–92.8	45.6–53.4
2017 Feb 15	28 (0)	400	1.11–1.08–1.25	85.4–106.8	45.4–59.2
2017 Feb 16	69 (49)	400	2.29–1.06–1.93	46.1–115.3	24.9–64.8
2017 Feb 17	27 (0)	400	1.81–1.23–1.07	67.5–95.4	39.0–55.5
2017 Mar 06	42 (0)	300	1.06–1.21–2.04	26.3–89.6	11.1–43.4
2017 Mar 7	93 (71)	300	2.23–1.06–2.41	48.6–83.1	26.1–45.5
2017 Mar 8	46 (0)	300	1.60–1.12–1.09	70.1–91.3	38.4–50.2

Notes. Number in parenthesis represents number of frames taken in-transit.

^a The signal-to-noise rate, S/N, is derived from the 16th order (585.03–591.62 nm) of the echelle spectrum, corresponding to the position of the sodium doublet line.

2.4. Telluric correction

As the next step, the Earth’s atmospheric signature needs to be accounted for. There are several ways to remove telluric lines from the spectra. One of the methods is to simultaneously observe an early-type rapidly rotating star to obtain the telluric spectrum. However, this method has a disadvantage of reducing the observing time spent on the primary target. Another method is described in Astudillo-Defru & Rojo (2013)

and Wyttenbach et al. (2015) where they use the fact that the variation of the telluric lines depth follows the airmass variation linearly. We decided to follow the method used in Casasayas-Barris et al. (2017). We took the 1D telluric spectrum constructed from the line list of HITRAN (Rothman et al. 2013) and matched its resolution to the resolution of the data. Then we corrected the reference telluric spectrum for the radial velocity to the same frame as the observed spectrum. The

telluric line’s absorption depth is changing with the airmass. Thus we used a least-squares method on the unblended telluric lines to scale the telluric model to the same airmass (depth) as the observed spectrum. Afterwards, we divided each observed spectrum by the telluric spectrum scaled for the given airmass using standard IRAF commands resulting in the removal of the telluric lines. As discussed in Casasayas-Barris et al. (2017), the scaling of the telluric spectra is not perfect as line depth variation is not equal for all the telluric lines, hence possibly introducing small residuals into the final transmission spectrum. As an illustration, the rms of a single-night transmission spectrum in the telluric region (589.9–590.4 nm) before applying the telluric correction is 0.00339. The rms of the same region was decreased to 0.00196 after applying the correction. For comparison, the rms of the spectral region without telluric features (587–587.5 nm) is 0.00193.

2.5. Transmission Spectrum

After the telluric correction, we averaged all out-of-transit spectra to create a “master out” frame, $\tilde{F}_{\text{out}}(\lambda) = \sum_{\text{out}} \tilde{f}_{\text{out}}(\lambda, t_{\text{out}})$. Next, we divided each in-transit frame $\tilde{f}_{\text{in}}(\lambda, t_{\text{in}})$ by $\tilde{F}_{\text{out}}(\lambda)$ to create the individual transmission spectra. Each of these frames was subsequently corrected for the planetary motion as the planetary signal is shifted from the stellar reference frame. We created a model of radial velocity taking only out-of-transit data.⁵ Finally, we summed up all the individual transmission spectra and normalized this sum to unity and then subtracted unity to retrieve the final transmission spectrum, $\tilde{\mathcal{R}}(\lambda)$, as

$$\tilde{\mathcal{R}}(\lambda) = \sum_{\text{in}} \frac{\tilde{f}_{\text{in}}(\lambda, t_{\text{in}})}{\tilde{F}_{\text{out}}(\lambda)} \Big|_{\text{Planet RV shift}} - 1. \quad (1)$$

2.6. Error Estimates

The uncertainties of the exo-atmospheric Na D lines measurements were estimated with a simple simulation from the data itself. This approach has the advantage of preserving as much as possible the systematic errors of the data.

The starting point of the simulation is our actual measurement—the fit that reproduces the observed spectrum with a flat line and two Gaussians (see Section 2.5). In the following we only consider a region of the spectrum containing 190 pixel elements, centered on the Na doublet. We converted the fit within this region into a noiseless spectrum with the same wavelength sampling as the original observational data.

The first step of our error analysis is to calculate the residuals of the observational data with respect to the fit. Second, the residuals were shifted by one pixel and then added to the best-fit model spectrum. Thus, the residual from the first pixel of the data was added to the second pixel of the fit, and the residual from the last pixel of the data was added to the first pixel of the best fit. This created a new realization of artificial data which have the same Na D signal and a different noise for each pixel. However, the overall statistical properties of the noise are preserved: for example if there is a systematic trend of increasing noise toward the end of the observations, because of

increasing airmass, it will be preserved. The third step is to remeasure the Na absorptions in the new artificial spectrum.

The last two steps were repeated 189 times, creating 189 unique new realizations—each time the shift of the residual pattern was increased by one, so for the second realization the first deviation was added to the third pixel and the last deviation was added to the second pixel. For the third realization the first deviation was added to the fourth pixel and the last deviation—to the third pixel. In general, to create the i th realization we added the first deviation to the $(i+1)$ th pixel of the noiseless model spectrum and the last realization—to the i th pixel of the noiseless model spectrum. Summarizing, this exercise is a simple shift of the residuals in a circular manner. It has been used before, e.g., by Cáceres et al. (2009, 2011).

The measurement errors were derived from the distributions (over all realizations) of the fitting parameters determined for each realization in the third step of the process described above. These distributions are shown in Figure 2. We adopt as final measurements and as their errors the means and the FWHM values of these distributions.

2.7. Stellar Activity

We also checked for possible false-positive detections. As suggested in Barnes et al. (2017), stellar activity could produce signatures in lines originating mainly from the stellar chromosphere. To rule out any such fake signals we investigated the vicinity of the Mg I (581.36 nm) and Ca I (612.22 and 616.22 nm) lines in Figure 3. The lack of any features in these regions shows that the increase of absorption in the sodium Na D lines is not caused by the chromospheric activity or by systematic effects in our analysis.

2.8. Rossiter–McLaughlin Effect

When looking at the presence of any atomic or molecular species in the spectrum of a planet, it is important to take into account the R–M effect (Queloz et al. 2000; Ohta et al. 2005), as shown by Wyttenbach et al. (2017). In Figure 4, we show the measured radial velocities of our targets as obtained with HARPS as well as the expected orbital motion of the star due to the presence of the planet. Any deviation from this could be due to the R–M effect. This is indeed the case for WASP-166, where the R–M effect is clearly visible (as also shown by Hellier et al. 2019). For the three other targets, the R–M effect is not measurable. It is possible to have an order of magnitude estimate of the R–M effect (Triaud 2018),

$$\Delta v_r \simeq \frac{2}{3} \gamma^2 V \sin i \sqrt{1 - b^2}, \quad (2)$$

where $V \sin i$ is the rotational velocity of the star, b is the impact parameter, and $\gamma = \frac{R_p}{R_s}$, with R_p being the radius of the planet and R_s that of the star. Estimating these values for the four targets we get the following values for Δv_r : 2.3 m s^{−1} (WASP-76), 2 m s^{−1} (WASP-127), 8 m s^{−1} (WASP-166), and 4 m s^{−1} (KELT-11). These are in agreement with what we see in Figure 4.

Moreover, in all cases, the R–M effect is too small to have any real impact on the depth of the Na D lines (Nortmann et al. 2018). We thus conclude here that the R–M effect is not important in our analysis.

⁵ As the planetary signal is shifted by as much as tens of kilometers from the rest frame, using the observed radial velocities would imply correcting for the possible R–M effect and would produce systematic effects in the final transmission spectrum (Cegla et al. 2017; Wyttenbach et al. 2017).

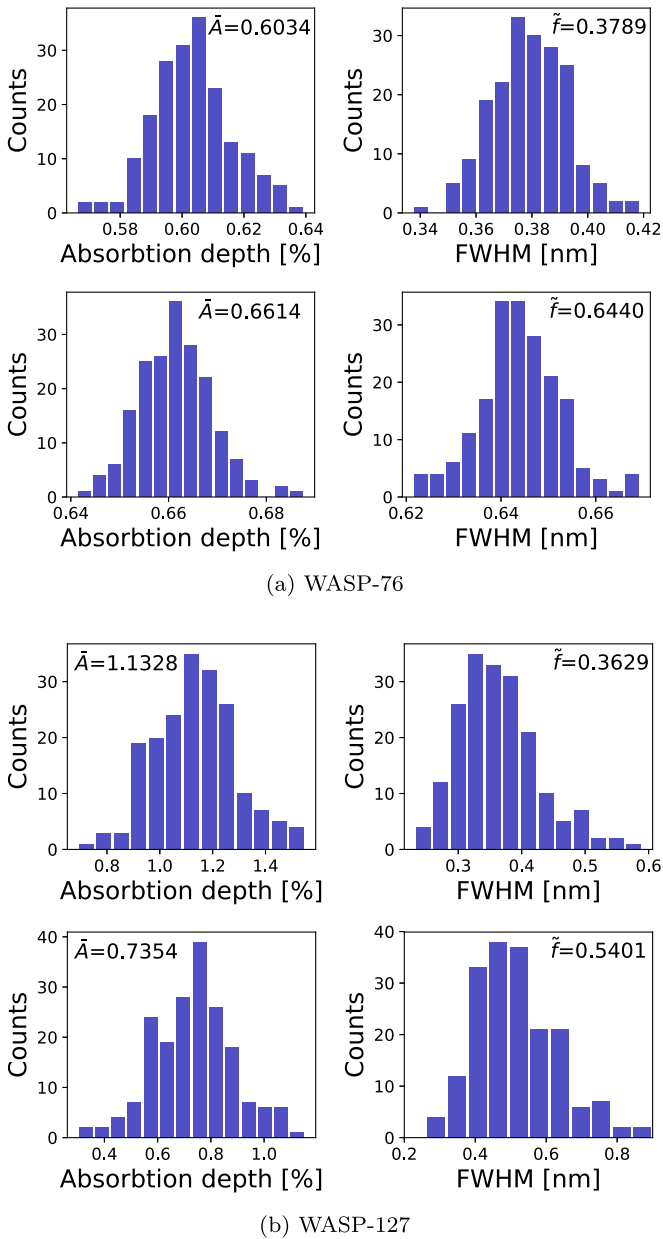


Figure 2. Distribution of the fitting parameters. The top rows of each subfigure show the parameter distribution for the D2 line while the bottom rows show the distribution for D1. Each plot displays the mean value. See the text for a description of the method.

3. Results

Each data set was analyzed for Na D, H_{α} , and H_{β} to see the absorption in the exo-atmosphere and for Ca I (612.2217 and 616.2173 nm) and Mg I (518.3604 nm) to monitor the stellar activity. The results are described for each star separately.

WASP-76b. The scale height of the atmosphere of WASP-76b is estimated to be about 1212 km, making it an excellent system for the analysis by transmission spectroscopy (Kabáth et al. 2019). This exoplanet was also suggested as one of the primary targets for *JWST* observations (Mollière et al. 2017). Figure 5 presents the final divided in-/out-of-transit spectra corrected for planetary radial velocity, displaying clearly visible planetary sodium (Na D lines) absorption. The rms of the Na D region is 0.0027 and the rms of the binned spectrum by 20 is 0.0013. The sodium line depths are 0.65% and 0.57%,

respectively, therefore, corresponding to 9.5σ and 7.1σ significance. This is an independent detection of sodium in the upper atmosphere of WASP-76b. Details of the detected peaks are summarized in Table 3.

Figure 3 shows the nonsignificant detections in the Ca I and Mg I lines (rms of the data points is 0.0007), showing that the stellar activity is low and any planetary atmosphere sodium (Na D lines) detection should be significant and not influenced by the star. Furthermore, the star WASP-76 is a slow rotator as reported by Brown et al. (2017).

The D1 line is apparently stronger than the D2 line, which would imply different mixing ratios and compositions of the atmospheres of different planets because all other detections reported were with a stronger D2 line. The explanation for the strength of the lines can be found in the literature for other Na lines in redder regions (Civiš et al. 2012), but such a measurement is missing in the optical. Civiš et al. (2012) present a laboratory spectrum of sodium lines demonstrating that different atomic states are shaping the spectral lines and their strengths. Furthermore, Slanger et al. (2005) measured the D2/D1 ratio in the Earth’s atmosphere and found it to be varying between 1.2 and 1.8. They explained that the variability of the ratio is originating from a competition between oxygen reacting with $\text{NaO}(A^3\Sigma^+)$, produced from the reaction of sodium with oxygen. In other words, the line strength and the mixing ratio depend on the composition of the surrounding atmosphere and it can even vary over time.

In the course of the review process of this paper, an independent detection of the sodium in the atmosphere of the WASP-76b planet by Seidel et al. (2019) was reported for the same HARPS data set. Their results are in agreement with ours, confirming the methodology. We note, however, that our FWHM of the D2 line is about 30% smaller compared to their values.

WASP-127b. WASP-127b is a heavily bloated super-Neptune. Its scale height is 2500 ± 400 km, making it another ideal target for transmission spectroscopy. Indeed, a cloudless sky was observed with many features such as sodium, potassium, and lithium detected and hints of TiO absorption were reported with Gran Telescopio Canarias (GTC) instrumentation (Pallé et al. 2017; Chen et al. 2018).

Figure 5 presents the final divided in-/out-of-transit spectrum. The rms of the data is 0.0042 and by binning by 20 points we reach a final rms of 0.0019. We were able to confirm only sodium (Na D lines) with a high significance of 4.2σ (D2) and 8.33σ (D1), respectively. We did not detect lithium (670.8 nm), which is most likely due to aperture differences between the GTC (10 m) and the 3.6 m telescope that hosts HARPS, while as mentioned earlier, potassium (766.5 and 769.9 nm) is out of range of HARPS. However, our confirmation of sodium is unique because this is one of the first proofs for observations using different instruments as well as two different methods. The stellar activity of the WASP-127 star can be monitored with the Ca I and Mg I lines. We were not able to see any activity in these lines, as shown in Figure 3.

WASP-166b. WASP-166b is a bloated super-Neptune with a scale height of 1103 km. Figure 5 presents the final divided in-/out-of-transit spectrum of all regions of interest. The rms of the data is 0.0025 and, after binning by 20, 0.0014. However, we are not able to detect any feature in the sodium (Na D) lines. Therefore, we can only put an upper limit of 0.14% on the detection.

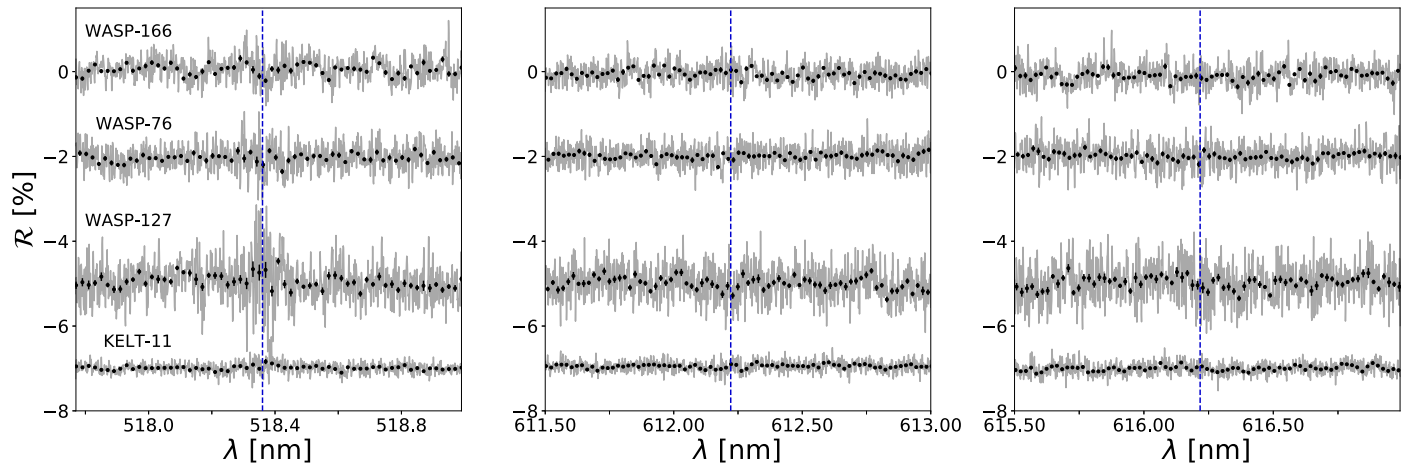


Figure 3. Activity cross-check region of the Ca I and Mg I lines for all of our targets. From left to right, the figure shows Mg I and both Ca I regions. Blue dashed lines indicate the exact position of the Mg I (518.3604 nm) and Ca I (612.2217 nm a 616.2173 nm) lines. The vertical offset was made for better readability.

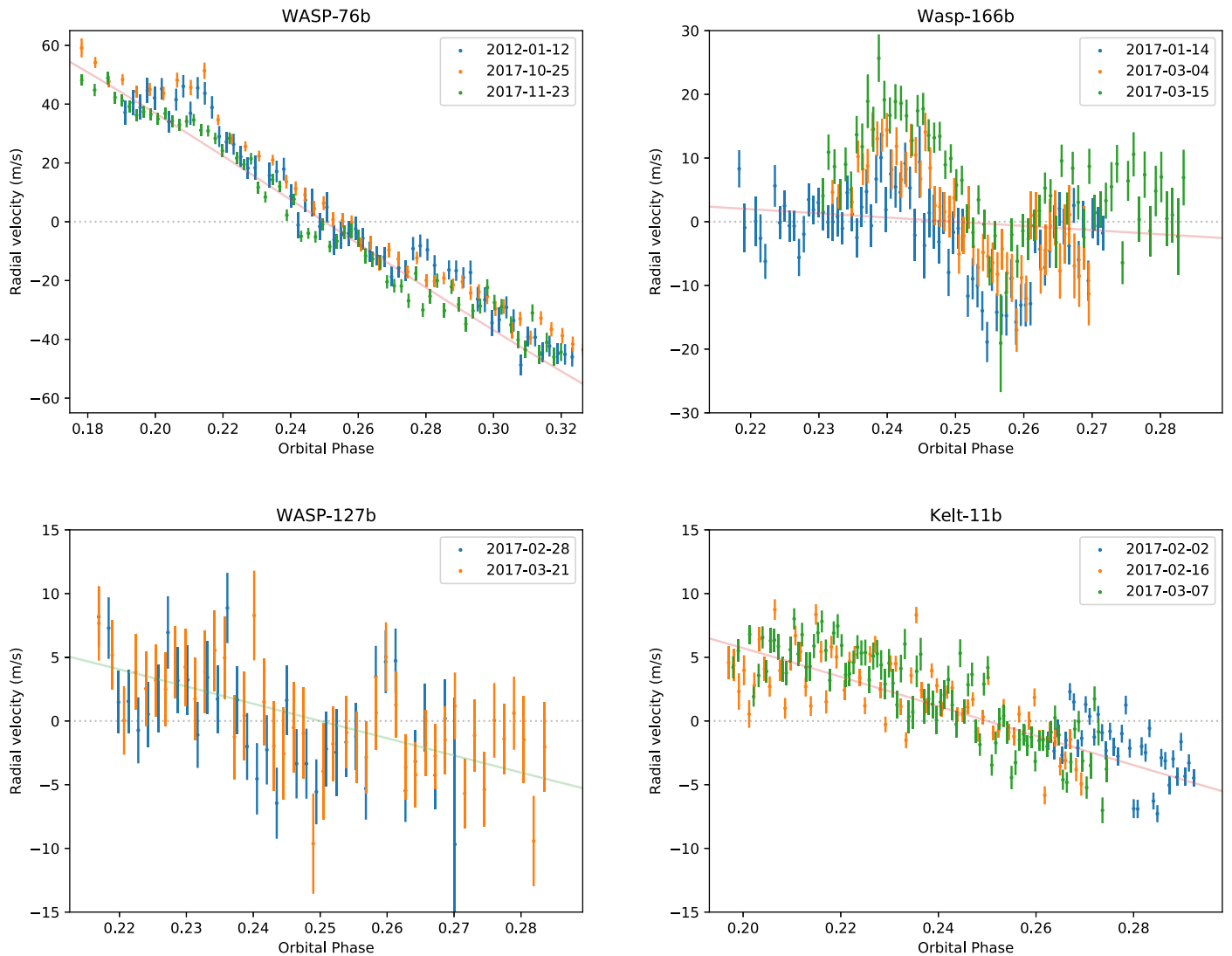


Figure 4. The radial velocities of our targets have been measured with HARPS: WASP-76 (top left), WASP-166 (top right), WASP-127 (bottom left), and KELT-11 (bottom right). There is some apparent offset between various epochs for the same target, which may be due to some instrumental shift or could be caused by the planet crossing star spots or faculae regions. In each case, the orbital motion is also indicated with the dashed line. Any deviation from this is due to the R–M effect, which is clearly in all but one of our targets.

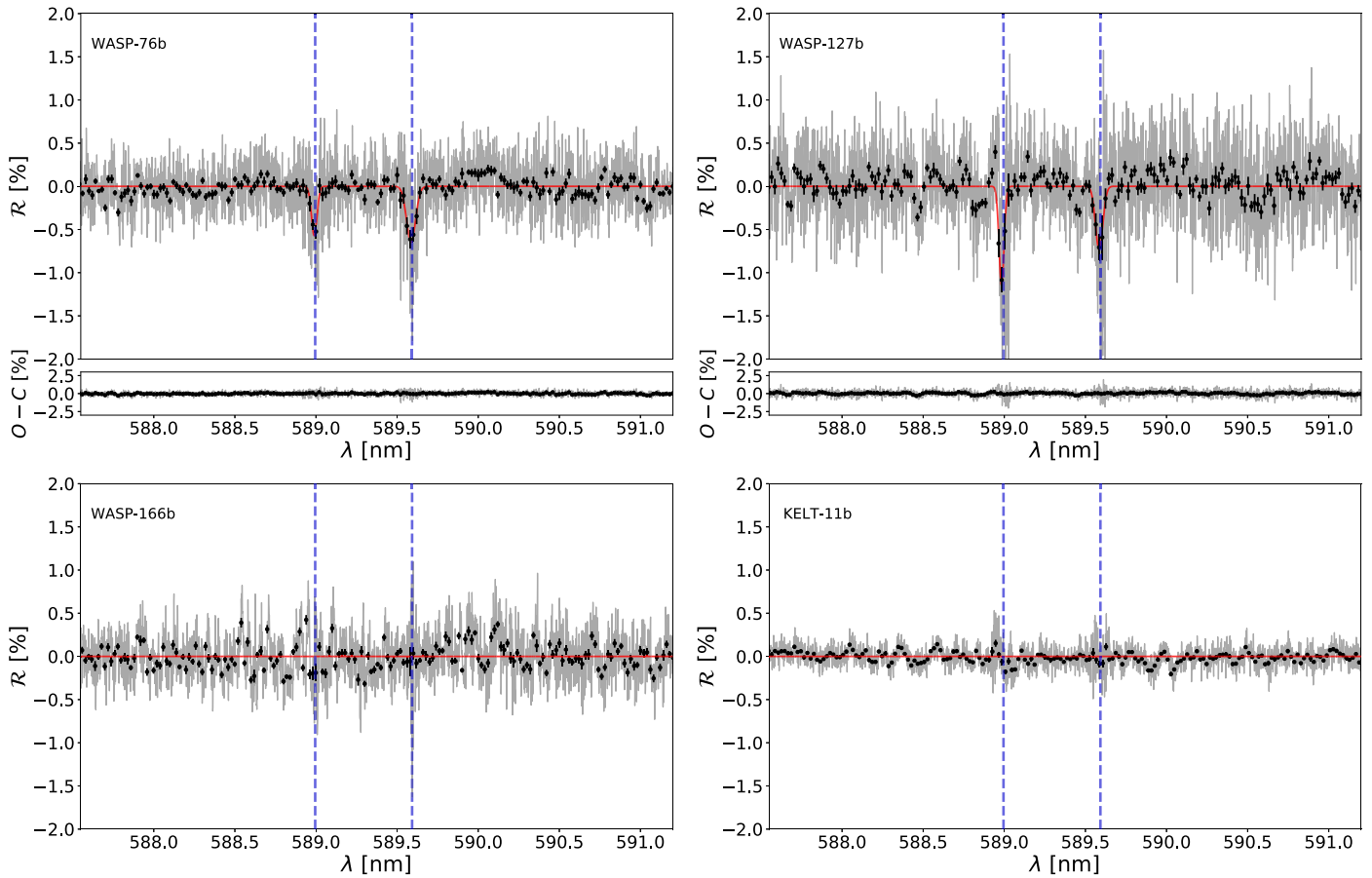


Figure 5. Spectral region around the sodium doublet for our four targets, removing the stellar signature. For WASP-76b (top left) and WASP-127b (top right), sodium is clearly detected, while for WASP166-b (bottom left) and KELT-11b (bottom right), nothing is evident. The blue dashed lines indicate the position of the Na D2 and D1 lines.

Table 3

Parameters Fits for the NaD Lines in WASP-76b and WASP-127b

Line	D1	D2
WASP-76b		
Depth (%)	0.648 ± 0.068	0.57 ± 0.08
FWHM (nm)	0.0650 ± 0.0078	0.0400 ± 0.0065
WASP-127b		
Depth (%)	0.735 ± 0.088	1.144 ± 0.270
FWHM (nm)	0.0537 ± 0.0075	0.0367 ± 0.0097

Table 4

Selected High-resolution Detections of Sodium (Na D Lines)

Planet	A_{D2}/A_{D1}	f_{D2}/f_{D1}
HD 189733b (1)	1.59 ± 0.33	1 ± 0.22
WASP-49b (2)	1.09 ± 0.47	1.91 ± 0.83
MASCARA-2b (3)	1.19 ± 0.39	0.79 ± 0.31
WASP-17b (4)	1 ± 0.66	1 ± 0.57
WASP-127b (5)	1.56 ± 0.41	0.68 ± 0.20
WASP-76b (5)	0.88 ± 0.15	0.62 ± 0.12

Figure 3 displays no signatures in the Mg I and Ca I lines. Therefore, we can assume that the star is not active.

KELT-11b. The scale height of KELT-11b is about 2500 km and since the planetary atmosphere is bloated, this is another excellent system for detection of an exo-atmosphere (Kabáth et al. 2019).

Figure 5 presents the final divided in-/out-of-transit spectrum of all regions of interest. The rms of the data is 0.0012 (unbinned) and 0.0006 (binned by 20 points). The upper limit for a sodium (Na D lines) detection is therefore 0.06%. This is a very stringent constraint on the presence of sodium in the atmosphere and possibly hints at the presence of clouds in the atmosphere of KELT-11b.

We checked the stellar activity on the Ca I and Mg I lines. There was no significant detection of activity observed in our data (see Figure 3).

Note. The first column states the exoplanet with the source of the values. The second column shows the ratio of the sodium doublet absorption lines. The third column shows the ratio of the sodium doublet FWHMs.

References. (1) Wyttenbach et al. (2015), (2) Wyttenbach et al. (2017), (3) Casasayas-Barris et al. (2018), (4) Khalafinejad et al. (2018), (5) this paper.

3.1. Previous Na D Detections

We have investigated all of the previous Na D line detections in exoplanets based on high-resolution spectroscopy. We have summarized them in Table 4. As can be seen, WASP-76b is the first reported planet having potentially an absorption ratio of D2 to D1 lines less than one.⁶

The unusual reported values make this planet an ideal target for future *JWST* follow-up to further clarify this discovery.

⁶ One should note, however, that the deviation from unity is less than 1σ , and we therefore do not claim much about this yet.

4. Conclusions

We investigated a group of four inflated gas giant planets, among which two inflated hot Jupiters and two super Neptunes. All four targets are ideal targets for transmission spectroscopy, given their magnitudes and their large scale heights. We reported an independent detection of sodium in WASP-76b with a $7-9\sigma$ significance.

We have been able to fully resolve the Na D lines. We report for the first time an absorption ratio of D2 to D1 lines less than one, although this is within 1σ of unity. If confirmed, this possibly hints at an unusual composition of the exo-atmosphere.

There was no hydrogen ($H\alpha$ and $H\beta$ lines) detected for WASP-76b. Another planet, WASP-127b was already characterized in previous studies and we could confirm the presence of sodium in the atmosphere. This is to our knowledge the first time such a detection is confirmed, and provides further credence to the transmission spectroscopy method given that two different instruments on two very different aperture telescopes (3.6 m versus 10 m GTC) provide similar results. For WASP-166b and KELT-11b, we were not able to detect any feature, despite having extremely precise data, thus hinting at cloudy skies or simply the absence of sodium and other elements. We note that nondetections are usually not reported, although they provide useful information as well.

The data presented here are available in the ESO archive under ESO Program IDs: 090.C-0540(F), 098.C-0304(A), and 0100.C-0750(A). P.K. and J.Z. would like to acknowledge the support from the GACR international grant 17-01752J. M.S. acknowledges financial support of Postdoc@MUNI project CZ.02.2.69/0.0/0.0/16_027/0008360. This work benefited from support for mobility by the DAAD-18-08 program, project ID: 57388159. We acknowledge the usage of IRAF and iSpec. We would like to thank the anonymous referee for providing comments that helped to improve the manuscript.

Software: HARPS Data Reduction Software, iSpec (Blanco-Cuaresma et al. 2014), IRAF (Tody 1986).

ORCID iDs

Jiří Žák  <https://orcid.org/0000-0001-9416-9007>

Petr Kabáth  <https://orcid.org/0000-0002-1623-5352>

Henri M. J. Boffin  <https://orcid.org/0000-0002-9486-4840>

Valentin D. Ivanov  <https://orcid.org/0000-0002-5963-1283>

Marek Skarka  <https://orcid.org/0000-0002-7602-0046>

References

- Allart, R., Bourrier, V., Lovis, C., et al. 2018, *Sci*, 362, 1384
 Allart, R., Bourrier, V., Lovis, C., et al. 2019, *A&A*, 623, A58
 Astudillo-Defru, N., & Rojo, P. 2013, *A&A*, 557, 56
 Barnes, J. R., Jeffers, S. V., Anglada-Escudé, G., et al. 2017, *MNRAS*, 466, 1733
 Birkby, J. L., de Kok, R. J., Brogi, M., et al. 2013, *MNRAS*, 436, L35
 Blanco-Cuaresma, S., Soubiran, C., Heiter, U., & Jofré, P. 2014, *A&A*, 569, 111
 Brown, D. J. A., Triaud, A. H. M. J., Doyle, A. P., et al. 2017, *MNRAS*, 464, 810
 Cáceres, C., Ivanov, V. D., Minniti, D., et al. 2009, *A&A*, 507, 481
 Cáceres, C., Ivanov, V. D., Minniti, D., et al. 2011, *A&A*, 530, 5
 Casasayas-Barris, N., Palte, E., Nowak, G., et al. 2017, *A&A*, 608, 135
 Casasayas-Barris, N., Palte, E., Yan, F., et al. 2018, *A&A*, 616, 151
 Cegla, H. M., Lovis, C., Bourrier, V., et al. 2017, *A&A*, 598, L3
 Charbonneau, D., Brown, T. M., Noyes, R. W., & Gilliland, R. L. 2002, *ApJ*, 568, 377
 Chen, G., Pallé, E., Nortmann, L., et al. 2017, *A&A*, 600, L11
 Chen, G., Pallé, E., Welbanks, L., et al. 2018, *A&A*, 616, 145
 Civiš, S., Ferus, M., Kubelík, P., et al. 2012, *A&A*, 542, 35
 Deibert, E. K., de Mooij, E. J. W., Jayawardhana, R., et al. 2019, *AJ*, 157, 58D
 Désert, J.-M., Vidal-Madjar, A., Lecavelier Des Etangs, A., et al. 2008, *A&A*, 492, 585
 Ehrenreich, D., Lecavelier Des Etangs, A., Hébrard, G., et al. 2008, *A&A*, 483, 933
 Gibson, N. P., Pont, F., & Aigrain, S. 2011, *MNRAS*, 411, 2199
 Hellier, C., Anderson, D. R., Triaud, A. H. M. J., et al. 2019, *MNRAS*, 488, 3067
 Jensen, A. G., Cauley, P., Redfield, S., Cochran, W. D., & Endl, M. 2018, *AJ*, 156, 154
 Jensen, A. G., Redfield, S., Endl, M., Cochran, W. D., et al. 2012, *ApJ*, 751, 86J
 Kabáth, P., Žák, J., Boffin, H., et al. 2019, *PASP*, 131, 085001
 Khalafinejad, S., Salz, M., Cubillos, P., et al. 2018, *A&A*, 618, 98
 Khalafinejad, S., von Essen, C., Hoeijmakers, H. J., et al. 2017, *A&A*, 598, 131
 Klocová, T., Czesla, S., Khalafinejad, S., et al. 2017, *A&A*, 607, A66
 Lam, K. W. F., Faedi, F., Brown, D. J. A., et al. 2017, *A&A*, 599, A3
 Lecavelier Des Etangs, A., Ehrenreich, D., Vidal-Madjar, A., et al. 2010, *A&A*, 514, 72
 Lendl, M., Cubillos, P. E., Hagelberg, J., et al. 2017, *A&A*, 606, 18
 Mayor, M., Pepe, F., Queloz, D., et al. 2003, *Msngr*, 114, 20
 Mollière, P., van Boekel, R., Bouwman, J., et al. 2017, *A&A*, 600, A10
 Murgas, F., Pallé, E., Parviainen, H., et al. 2017, *A&A*, 605, 114
 Nortmann, L., Pallé, E., Salz, M., et al. 2018, *Sci*, 362, 1388
 Ohta, Y., Taruya, A., & Suto, Y. 2005, *ApJ*, 622, 1118
 Oshagh, M., Triaud, A. H. M. J., Burdanov, A., et al. 2018, *A&A*, 619, A150
 Pallé, E., Chen, G., Prieto-Arranz, J., et al. 2017, *A&A*, 602, L15
 Pearson, K. A., Griffith, C. A., Robert, T. Z., et al. 2019, *AJ*, 127, 21P
 Pepper, J., Rodriguez, J. E., Collins, K. A., et al. 2017, *AJ*, 153, 215
 Queloz, D., Eggenberger, A., Mayor, M., et al. 2000, *A&A*, 359, L13
 Redfield, S., Endl, M., Cochran, W. D., & Koesterke, L. 2008, *ApJL*, 673, L87
 Ricker, G. R., Winn, J. N., Vanderspek, R., et al. 2015, *JATIS*, 1, 014003
 Rothman, L. S., Gordon, I. E., Babikov, Y., et al. 2013, *JQSRT*, 130, 4
 Sedaghati, E., Boffin, H. M. J., Csizmadia, S., et al. 2015, *A&A*, 576, L11
 Sedaghati, E., Boffin, H. M. J., Jeřabková, T., et al. 2016, *A&A*, 596, A47
 Sedaghati, E., Boffin, H. M. J., MacDonald, R. J., et al. 2017, *Natur*, 549, 238
 Seidel, J. V., Ehrenreich, D., Wytenbach, A., et al. 2019, *A&A*, 623, A166
 Slander, T., Cosby, T., Huestis, D. L., et al. 2005, *JGR*, 110, D23302
 Snellen, I. A. G., Albrecht, S., de Mooij, E. J. W., et al. 2008a, *A&A*, 487, 357
 Snellen, I. A. G., de Kok, R. J., de Mooij, E. J. W., & Albrecht, S. 2008b, *Natur*, 465, 1049
 Spake, J. J., Sing, D. K., Evans, T. M., et al. 2018, *Natur*, 557, 68
 Swain, M. R., Vasisht, G., & Tinetti, G. 2008, *Natur*, 452, 329
 Tinetti, G., Vidal-Madjar, A., Liang, M.-C., et al. 2007, *Natur*, 448, 169
 Tody, D. 1986, *Proc. SPIE*, 627, 733
 Triaud, A. H. M. J. 2018, in *Handbook of Exoplanets*, ed. H. Deeg & J. Belmonte (Cham: Springer), 1375
 Vidal-Madjar, A., Lecavelier des Etangs, A., Désert, J.-M., et al. 2003, *Natur*, 422, 143
 West, R. G., Hellier, C., Almenara, J.-M., et al. 2016, *A&A*, 585, 126
 Wytenbach, A., Ehrenreich, D., Lovis, C., Udry, S., & Pepe, F. 2015, *A&A*, 577, 62
 Wytenbach, A., Lovis, C., Ehrenreich, D., et al. 2017, *A&A*, 602, 36